RSC Applied Interfaces

ROYAL SOCIETY OF CHEMISTRY

PAPER

View Article Online
View Journal | View Issue

Open Access Article. Published on 25 Fankwa-b 2023. Downloaded on 2025/10/07 3:46:55 AM.
This article is licensed under a Creative Commons Attribution 3.0 Unported Licence.

Check for updates

Cite this: *RSC Appl. Interfaces*, 2024, **1**, 147

Al(III)-based MOF for the selective adsorption of phosphate and arsenate from aqueous solutions†

Juan L. Obeso,[ab] Herlys Viltres,[c] Catalina V. Flores,[ab] Valeria B. López-Cervantes,[b] Camilo Serrano-Fuentes,[a] Amin Reza Rajabzadeh,[c] Seshasai Srinivasan,[c] Ricardo A. Peralta,*[d] Ilich A. Ibarra*[be] and Carolina Leyva*[a]

Received 30th May 2023,
Accepted 15th September 2023

DOI: 10.1039/d3lf00061c

rsc.li/RSCApplInter

The occurrence of harmful ions in water can damage ecosystems and human health. For this, we reported an Al(III)-based MOF (DUT-5), which was synthesized *via* the solvothermal method and applied to remove phosphate and arsenate from aqueous solutions. DUT-5 displayed high adsorption capacity and stability in the pH range from 4 to 9, besides a high selectivity for phosphate removal and outstanding reusability. The maximum adsorption capacities for phosphate and arsenate were 233.26 and 131.32 mg g^{-1}, respectively. The modeling of the experimental data indicated that chemical forces were involved in the adsorption process since this followed the PSO and Freundlinch models. In addition, the mechanism was elucidated by FTIR and XPS analysis, confirming the possible interactions of the arsenate and phosphate with DUT-5 during the adsorption process. Hydrogen bonding and electrostatic interactions were exhibited for arsenate and hydrogen bonding for phosphate removal. Furthermore, this study confirms that DUT-5 is a suitable adsorbent, significantly contributing to water treatment.

Introduction

The high impact of water pollution on public health and the environment has generated significant concern in our modern society.[1] In the last century, a substantial amount of contaminated water has been discharged, mostly into rivers, lakes, and oceans. The most important contaminants are derived from anthropogenic activities such as industry, agriculture, and mining.[2] Water pollutants mainly involve heavy metals, pesticides, pharmaceuticals, dyes, pathogens, suspended solids, and nutrients.[3]

Among the various existing pollutants, arsenic and phosphorus have emerged as global environmental challenges based on their hazardous nature.[4,5] Arsenic is considered part of heavy metals for its high toxicity. Also, this pollutant exhibits different negative effects on human health, such as the increased risk of cancer, cardiorespiratory disorders, repercussions on the reproductive system, and cognitive impact.[6] On the other hand, phosphorus is one of the major nutrients, which, at high concentrations, represents a significant danger. The main effect is the generation of eutrophication, causing uncontrolled growth of microalgae, phytoplankton, and plants,[7] and their presence on the water's surface inhibits photosynthesis and leads to an oxygen deficit.[8]

Different techniques have been developed for treating these pollutants using various processes, such as degradation,[9] microfiltration,[10] coagulation–flocculation,[11] and adsorption.[12] Although the most commonly used strategy for water treatment is the implementation of solid-state adsorbent materials for their low cost, environmental sustainability, and recyclability. Traditional adsorbents, such as activated carbons,[13] zeolites,[14] and biomass,[15] have been broadly applied. However, these materials have certain disadvantages, such as low adsorption capacity, difficult separation, and instability, and thereby, novel strategies have been implemented to alleviate these issues.

MOFs are crystalline inorganic–organic hybrid materials constructed by self-assembling metal ions or clusters as nodes and organic linkers as connectors.[16] MOFs are chemically and

[a] *Instituto Politécnico Nacional, CICATA U. Legaria, Laboratorio Nacional de Ciencia, Tecnología y Gestión Integrada del Agua (LNAgua), Legaria 694, Col. Irrigación, Miguel Hidalgo, 11500, CDMX, Mexico. E-mail: zleyva@ipn.mx*
[b] *Laboratorio de Fisicoquímica y Reactividad de Superficies (LaFReS), Instituto de Investigaciones en Materiales, Universidad Nacional Autónoma de México, Circuito Exterior s/n, CU, Coyoacán, 04510, Ciudad de México, Mexico. E-mail: argel@unam.mx*
[c] *School of Engineering Practice and Technology, McMaster University, 1280 Main Street West Hamilton, ON, L8S 4L8, Canada*
[d] *Departamento de Química, División de Ciencias Básicas e Ingeniería, Universidad Autónoma Metropolitana (UAM-I), 09340, Mexico. E-mail: rperalta@izt.uam.mx*
[e] *On sabbatical as "Catedra Dr. Douglas Hugh Everett" at Departamento de Química, Universidad Autónoma Metropolitana-Iztapalapa, San Rafael Atlixco 186, Col. Vicentina, Iztapalapa, C.P. 09340, Ciudad de México, Mexico*

† Electronic supplementary information (ESI) available: Instrumental techniques, characterization, and experimental data. See DOI: https://doi.org/10.1039/d3lf00061c

Open Access Article. Published on 25 Fankwa-b 2023. Downloaded on 2025/10/07 3:46:55 AM.
This article is licensed under a Creative Commons Attribution 3.0 Unported Licence.

thermally stable at high temperatures, with high adsorption capacity, surface area, and uniform pore size distribution.[17] These salient characteristics have resulted in their applications in several fields, such as drug delivery,[18] adsorption,[19] catalysis,[20] and detection.[21] Also, MOFs have been tested for organic and inorganic pollutant adsorption in water remediation.[22–24] Mainly, arsenic and phosphate adsorption has been under study. For example, for arsenic adsorption, UiO-66 showed low adsorption capacity (89.3 mg g^{-1}). However, as the material was modified with defects in its structure, the adsorption capacity increased (138.4 mg g^{-1}).[25] On the other hand, MIL-100(Fe),[26] and MIL-53(Al),[27] were studied for arsenic adsorption, showing poor adsorption capacity, and mostly arsenic was coordinated in the structure, decreasing the possibility of reusing the material. The amino-functionalized MIL-101(M) (M = Al, and Fe) also displayed high phosphate adsorption capacity. However, the strong host-adsorbent interaction causes a ligand exchange.[28] Nevertheless, the modification in pristine MOFs increased the cost of synthesis, which generally complicates their applications on an industrial scale. Consequently, the implementation of functionalized MOF materials for the efficient removal of these contaminants, of simple synthesis and low-cost synthesis, is required.

DUT-5 is a prominent material formed from a large abundance of metal sources. The low cost and less toxic nature of aluminum leads to the chemistry of Al-based MOFs being of special interest.[29] The material's composition consists of hydroxo-functionalized (μ_2-OH) and infinite Al(III)–oxygen octahedra forming (–Al–OH–) chains linked to 4,4′-biphenyl dicarboxylate (BPDC) linker.[30] In our previous research, DUT-5 showed high adsorption capacities for dyes and pharmaceutical products.[31,32] Buoyed, DUT-5 was evaluated for water remediation in arsenate and phosphate adsorption. The optimization, adsorption kinetics, isotherms, structure stability to water, and reusability of DUT-5 were studied in the present work. Moreover, FTIR and XPS techniques were used to determine the main adsorption mechanism of the arsenate and phosphate. The reusability was evaluated over multiple cycles. This study sets DUT-5 as a possible candidate to be applied as an adsorbent for water treatment focused on phosphate and arsenate removal.

Experimental

Chemicals

Nonahydrate aluminum nitrate ($Al(NO_3)_3{\cdot}9H_2O$, 98%), 4,4′-biphenyl dicarboxylic acid (H_2BPDC, 95%), *N*,*N*-dimethylformamide (DMF, 99.8%), high purity deionized water with specific resistance of 18 mΩ cm^{-1} was obtained from a Mili-Q system Simplicity®, sodium bicarbonate ($NaHCO_3$, 98%), sodium arsenate dibasic heptahydrate ($Na_2HAsO_4{\cdot}7H_2O$, 98%), potassium phosphate monobasic (KH_2PO_4, 99%), sodium carbonate (Na_2CO_3, 99.5%), sodium chloride (NaCl, 99%), sodium hydroxide pellets (NaOH, 97%), and hydrochloric acid (HCl, 37%) were supplied by Sigma-Aldrich. All reagents and solvents were used as received from commercial suppliers without further purification.

Synthesis of DUT-5

The synthesis of DUT-5 was performed as reported by Kaskel and co-workers.[30] First, BPDC linker (0.26 g, 1.07 mmol) and $Al(NO_3)_3{\cdot}9H_2O$ (0.52 g, 1.4 mmol) were dissolved in DMF (30 mL). Next, the mixed solution was added to a Teflon liner placed in an autoclave (50 mL), then heated to 120 °C for 24 h. Subsequently, the powder was washed with DMF (three times) and dried at 100 °C overnight.

Instruments

Detailed information on the instrumental techniques is available in section S1.†

Adsorption experiments

The adsorption studies were conducted at room temperature. The optimization parameters were varied for mass, pH, initial concentration, temperature, contact time, and reusability (see ESI†). Each experiment was carried out with 30 mL of arsenate or phosphate solution at a specific concentration. The conditions were adjusted accordingly to understand the effect of experimental parameters. After adsorption, the material was separated by centrifugation (4000 rpm for 6 min). Initial and residual arsenate concentrations were determined using an Inductively Coupled Plasma Mass Spectrometer Optima 8000 (ICP-OES, Perkin Elmer, United States) as total arsenic content. Phosphate analysis was performed in a UPLC Acquity system, which consists of a quaternary pump coupled to an FTN auto-sampler, an isocratic solvent manager, and a 2432 conductivity detector from Waters™. Samples were separated on an IC-Pack™ Anion HR (4.6 × 75 mm) column at 35 °C with isocratic elution (0.7 mL min^{-1}). The mobile phase composition was 3 mM $NaHCO_3$/2.4 mM Na_2CO_3. In addition, an anion chemically regenerated suppressor Dionex™ ACRS 500 (4 mm) from Thermo Scientific was installed between the detector and the separation column, using a 200 mN H_2SO_4 solution as a chemical regenerator with a flow of 0.5 mL min^{-1}, to increase the detector sensitivity. With these conditions, the retention time for phosphate was around 8.5 min, with a total run time for each sample of 10 min. The adsorbent reusability was studied for three adsorption–desorption cycles. The kinetic data were fitted to four models: pseudo-first order (PFO), pseudo-second order (PSO), Elovich, and intraparticle, defined in Table S1.† The adsorption data were fitted to three isotherms models: the Langmuir, the Freundlich, and the Temkin, described in Table S2.†

Results and discussion

Characterization of DUT-5

PXRD pattern of DUT-5 (Fig. S1†) proves the purity of the phase, which is similar to the reported with signature peaks of 2θ at 5.93°, 12.05°, 14.08° and 18.11°.[30] FTIR confirms the

 © 2024 The Author(s). Published by the Royal Society of Chemistry

Open Access Article. Published on 25 Fankwa-b 2023. Downloaded on 2025/10/07 3:46:55 AM.
This article is licensed under a Creative Commons Attribution 3.0 Unported Licence.

presence of the main functional groups (Fig. S2†). The absorption bands of the carboxylate group coordinated to the metal center are at 1601 and 1428 cm^{-1} for asymmetric and symmetric stretching vibration, respectively.[33] From the N_2 adsorption–desorption isotherm (Fig. S3†), the surface BET area and pore volume were calculated (1616 m^2 g^{-1} and 0.55 cm^3 g^{-1}), consistent with the reported data.[30,34] The thermal stability was confirmed using TGA analysis (Fig. S4†), showing strength up to 430 °C. Moreover, these techniques corroborated the successful DUT-5 characterization.

Parameter optimization: adsorbent mass, time, pH, and concentration effect on adsorption

The stability of DUT-5 in water and different pH (from 4 to 9) was confirmed by PXRD. The crystalline structure was retained after the test (Fig. S5†). The BET surface area was retained (1605 m^2 g^{-1}) after the stability test (Fig. S6†). Initially, the effect of adsorbent dosage on adsorption was studied in the range of 5–20 mg for both ions (Fig. 1a). The adsorption capacity decreased with the increase of the adsorbent dosage for both contaminants. Noticeably, the number of adsorption sites rises according to the increment in mass, indicating that DUT-5 possesses available adsorption sites.[35]

The arsenate and phosphate adsorption capacity from aqueous solutions as a function of contact time was studied for 24 h (Fig. 1b). The adsorption capacity increased rapidly in the first hour (60 min) for phosphate and the second hour (120 min) for arsenate. Therefore, a consistently high concentration of ions and multiple available adsorption sites contributed to a rapid mass transfer.[36] Additionally, the fast adsorption could be related to a stronger diffusion of the ions into the channels of the DUT-5. The adsorption capacity equilibrium was reached at around 480 and 720 min for phosphate and arsenate, respectively. As a result, the maximum adsorption capacity was 73.3 and 45.0 mg g^{-1} for phosphate and arsenate, respectively.

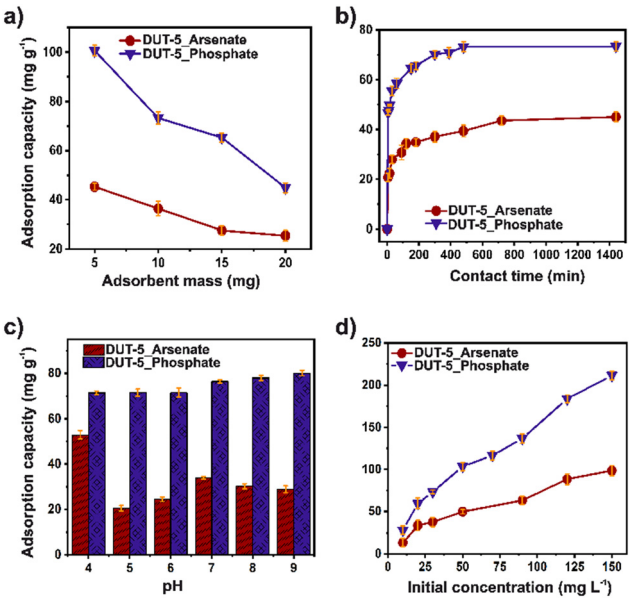

Fig. 1 Effect of the a) adsorbent dosage, b) pH, c) pollutant initial concentration, and d) the contact time on the arsenate (red) and phosphate (blue) adsorption over DUT-5.

The pH also plays an important role in adsorption, especially in the change in the surface polarity of the MOF and the distribution and speciation of arsenate and phosphate ions. Thus, the effect of pH on the adsorption capacity of both pollutants in the aqueous solutions was investigated for a pH range of 4–9 (Fig. 1c). From this, the isoelectric point of DUT-5 is 6.4 (Fig. S7†), where a higher value, the surface is charged negatively, and at lower values are positive. It is observed that at pH 9, a high removal of phosphate can be reached and a slight improvement in the adsorption capacity. Since the chemical speciation of phosphate is HPO_4^{2-} at pH 9 (Fig. S8†), and the DUT-5 surface is negative, the electrostatic interactions are negligible.[37] For arsenate adsorption, the chemical speciation (Fig. S9†) is H_3AsO_4 (at pH < 2.1), $H_2AsO_4^-$ ($2.1 <$ pH < 6.7), and $HAsO_4^{2-}$ (pH > 6.7).[25] The adsorption capacity decreased close to the isoelectric point of DUT-5, while at pH 4, the removal was enhanced. It is directly related to the positive surface and anionic species of arsenic, mainly due to electrostatic interactions.

The influence of phosphate and arsenate concentration on the adsorption was explored in the range of 10–150 mg L^{-1} for both ions (Fig. 1d). The adsorption capacity from aqueous solutions was increased as the increasing concentration and achieved the highest value of 98.58 and 211.43 mg g^{-1} for arsenate and phosphate, respectively. DUT-5 exhibits outstanding adsorption capacity for both ions even in a high-concentration solution (150 mg L^{-1}), confirming the availability of abundant adsorption sites. In addition, the surface changes in the morphology after the adsorption process for both pollutants were monitored using SEM (Fig. S11†). DUT-5 shows a lumpy sheet-like interconnected structure with a homogeneous morphology. No apparent changes are observed after the adsorption process.

Since DUT-5 displays high water stability and an easy synthesis route, the adsorption capacity for arsenate and phosphate using DUT-5 was compared with different MOFs, and the summary can be observed in Table S3.† In addition, for arsenate, DUT-5 outperforms UiO-66,[25] MIL-100(Fe),[26] MIL-53(Al),[27] and MOF-808.[38] On the other hand, DUT-5 exhibits outstanding performance for phosphate adsorption. It is noted that DUT-5 is exceeding to Ce-BDC,[39] HP-UiO-66(Zr),[40] NH_2-MIL-101(X, X = Al and Fe),[28] Gd-PTA,[41] and Fe–Al-MOF.[37]

Adsorption kinetics and isotherms

To establish the kinetics process of the arsenate and phosphate adsorption, pseudo-first order (PFO), pseudo-second order (PSO), Elovich, and intra-particle diffusion

Open Access Article. Published on 25 Fankwa-b 2023. Downloaded on 2025/10/07 3:46:55 AM.
This article is licensed under a Creative Commons Attribution 3.0 Unported Licence.

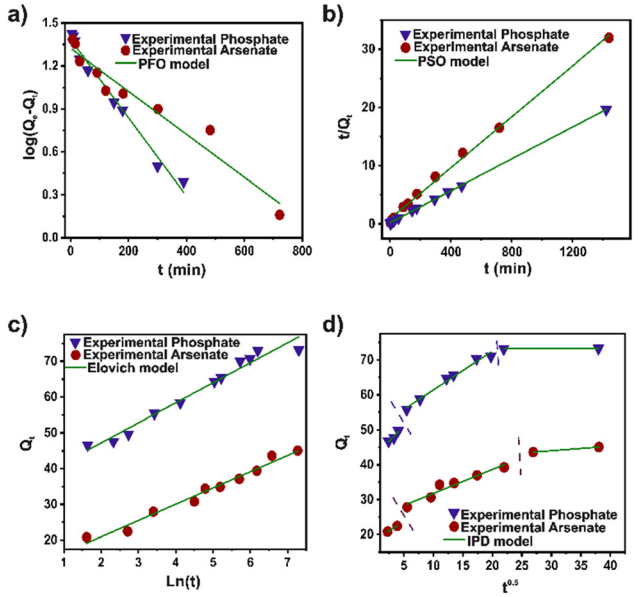

Fig. 2 Kinetics fits for phosphate (blue) and arsenate (red) adsorption using DUT-5 as adsorbent: a) pseudo-first-order (PFO), b) pseudo-second-order (PSO), c) Elovich, and d) intra-particle diffusion (IPD).

(IPD) models were used to fit the experimental data (Fig. 2). The kinetic parameters for the models are illustrated in Table S4.† Based on the correlation coefficient (R^2), the experimental data for arsenate and phosphate were fixed properly for the four kinetic models. However, the PSO model displays the highest R^2 for both pollutants. A broadly consistent theoretical adsorption capacity (45.6 and 73.7 mg g^{-1}) is noted, with the experimental data (73.3 and 45.0 mg g^{-1}) for arsenate and phosphate, respectively. This strongly implies that the adsorption capacity depends primarily on the available adsorption sites. This model suggested that a chemical interaction in a heterogeneous surface is the controlled step in the adsorption process.[42] The pseudo-second-order rate constant (K_2) value for phosphate was twice that of the arsenate. This can be attributed to the rapid adsorption, mainly to its high surface area and adequate pore distribution in DUT-5. Nevertheless, the IPD model also shows an adequate R^2 parameter in the fit for both cases. Evidently, the diffusion process is part of the rate-controlling step for adsorption. The second step in the IPD model assumed a gradual adsorption rate. The stage intercept (C_2) of the boundary layer of adsorption shows around 55–60% of the total adsorption capacity for both pollutants until it reaches complete equilibrium. Also, the rate parameter of the stage (K_{ip2}) corroborated the high molecule diffusion for the bulk solution to the material.[43]

In addition, Langmuir, Freundlich, and Temkin models were applied to analyze the phosphate and arsenate adsorption data (Fig. 3). Isotherms parameters are presented in Table S5.† It was noted that the Freundlich model fits adequately for both pollutants to describe the adsorption performance. The R^2 was 0.9512 and 0.9854 for arsenate and phosphate adsorption, respectively. Freundlich model infers a heterogeneous

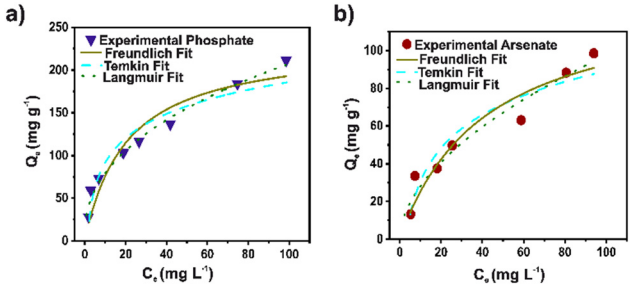

Fig. 3 Langmuir, Freundlich, and Temkin isotherm fit for a) phosphate (blue) and b) arsenate (red) using DUT-5.

adsorption surface—leading multilayer adsorption with different adsorption sites on the surface.[44] Similarly, the adsorption intensity (n^{-1}) is below 1; therefore, the adsorption processes can be described as favorable. Moreover, based on the Langmuir fit, the maximum adsorption capacity was 131.32 and 233.26 mg g^{-1} for arsenate and phosphate, respectively. Outstanding, the maximum adsorption capacity for phosphate adsorption is one of the highest values for MOF materials. In addition, the value of the separation factor (R_L) was in the interval lower than 1, and the free Gibbs energy was negative. This corroborated a promising adsorption process for both pollutants.[45]

Effect of temperature and coexistence ions

The effect of temperature is observed in Fig. 4a. It is evident that the adsorption capacity improves for both pollutants

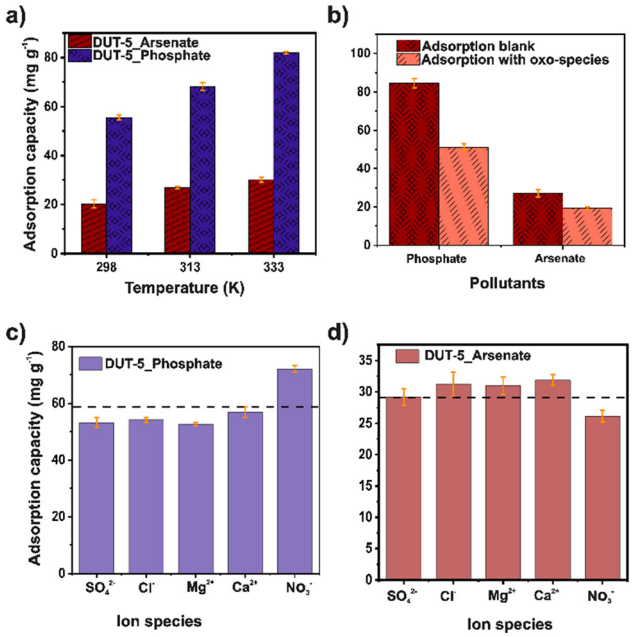

Fig. 4 a) Effect of temperature on phosphate and arsenate adsorption, b) phosphate and arsenate competition, c) effect of coexistent ions for phosphate adsorption, and d) effect of coexistent ions for arsenate adsorption.

 © 2024 The Author(s). Published by the Royal Society of Chemistry

Open Access Article. Published on 25 Fankwa-b 2023. Downloaded on 2025/10/07 3:46:55 AM.
This article is licensed under a Creative Commons Attribution 3.0 Unported Licence.

with increasing temperature. Moreover, this behavior is attributed to the change in kinetic energy because the motion of the particles increases, which enhances the adsorbate–adsorbent interactions.[46] Thus, free energy ($\Delta G°$), enthalpy ($\Delta H°$), and entropy ($\Delta S°$) parameters were calculated using the van't Hoff plot (Fig. S10†).[47] The thermodynamics parameters are shown in Table S6.† For both pollutants, $\Delta G°$ was negative in the three temperatures, indicating a viable and spontaneous process. The relatively low and positive $\Delta H°$ values (15.26 and 37.05 kJ mol^{-1}, for arsenate and phosphate, respectively) demonstrate an endothermic adsorption process. The differences in these values may be associated with arsenate removal since electrostatic interactions are the dominant interaction in the mechanism, consistent with the pH analysis. Also, the positive $\Delta S°$ value suggests a higher material disorder at the solid–liquid interface.[38]

Additionally, the phosphate and arsenate competition effects were tested (Fig. 4b). First, the competition was evaluated only in the presence of phosphate and arsenate. It was observed that DUT-5 exhibits high selectivity for phosphate. On the other hand, the selectivity experiments were performed in the presence of other oxo-species, such as dichromate, permanganate, and perchlorate. In this case, DUT-5 still shows a high adsorption capacity for phosphate.

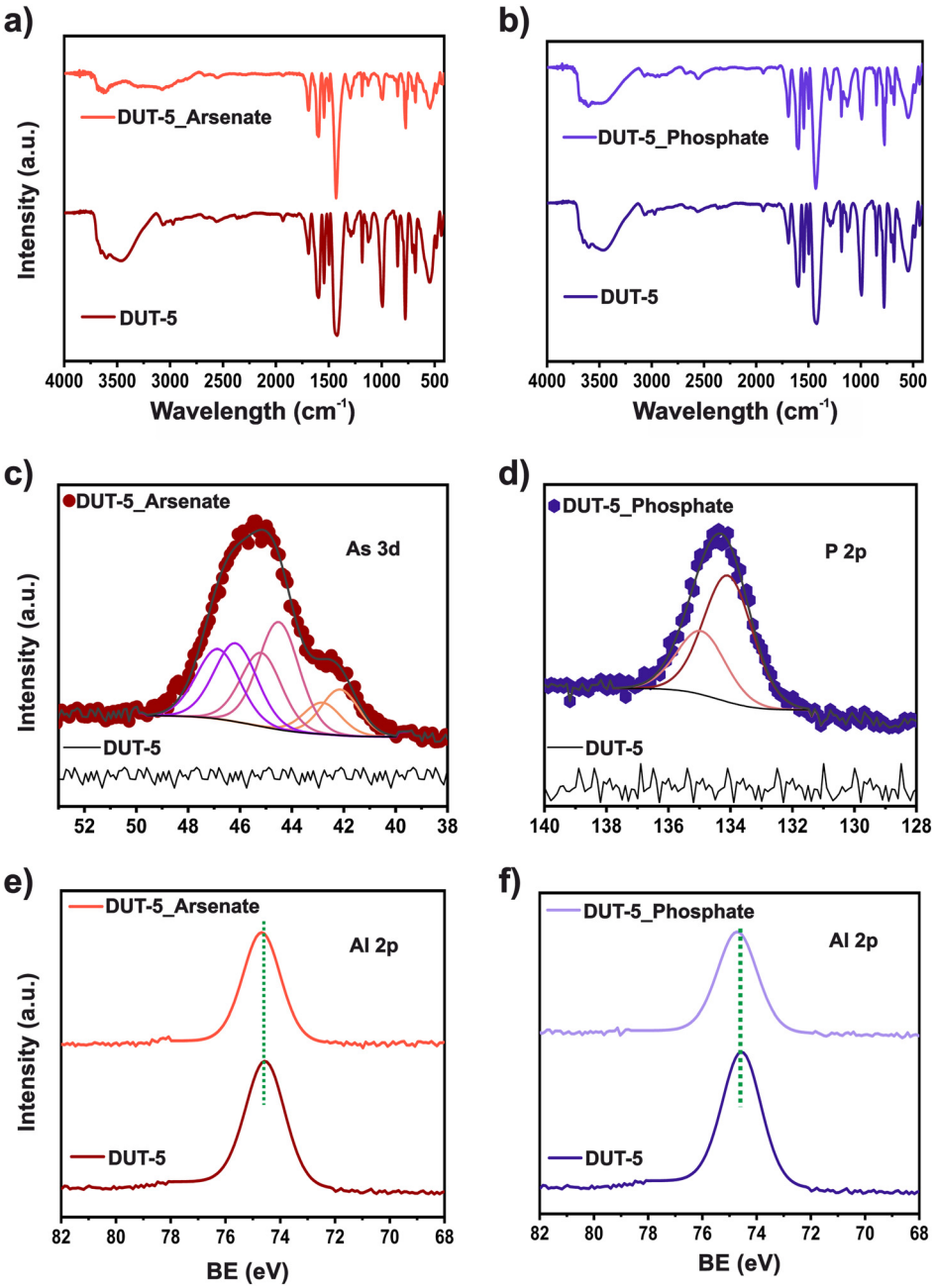

Fig. 5 (a and b) FTIR spectra; c) As 3d HRXPS; d) P 2p; (e and f) Al 2p spectra of DUT-5 before and after arsenate and phosphate adsorption.

Open Access Article. Published on 25 Fankwa-b 2023. Downloaded on 2025/10/07 3:46:55 AM.
This article is licensed under a Creative Commons Attribution 3.0 Unported Licence.

The adsorption capacity only drops 40% compared to the blank experiment due to the competition for adsorption sites generated by the presence of additional oxo-ions. Also, the impact of coexistence ions in the adsorption process was evaluated (Fig. 4c and d). One milliequivalent of SO_4^{2-}, Cl^-, Mg^{2+}, Ca^{2+}, and NO_3^- was used for this study. The adsorption capacity decreased except when NO_3^- was present in the solution for phosphate adsorption. On the other hand, the performance is the opposite for arsenate adsorption. This can be attributed to the fact that an ion competition is performed due to the electrostatic interaction. Mainly, in competition experiments lead to modifying the adsorption capacity for both pollutants.[48]

Adsorption mechanism

The possible phosphate and arsenate adsorption mechanism on DUT-5 adsorbent was analyzed using FTIR and XPS spectroscopy (Fig. 5). FTIR spectra of DUT-5 before and after arsenate (Fig. 5a) and phosphate (Fig. 5b) adsorption, display changes in the absorption bands intensities. Furthermore, after removing both pollutants, a decrease in the intensity of the main functional groups' signals is observed. This suggests that these sites are involved in pollutant adsorption.[45]

An XPS analysis was conducted to gain further insights into the adsorption mechanism. High-resolution (HR) spectra regions for DUT-5 before and after arsenate and phosphate adsorption are shown in Fig. 5c–f. Before adsorption, no signals corresponding to As 3d or P 2p for DUT-5 are observed. However, after adsorption, clear signals of As 3d and P 2p are noted for the presence of arsenate and phosphate, respectively, within the material. HRXPS As 3d spectrum displays contributions at 44.1, 44.5, and 46.2 eV. These signals are designated to As $3d_{5/2}$ peak of two –As(III)–O and one –As(V)–O contributions, respectively. The conditions of XPS measurements could cause part of the reduced As in the sample. It was reported that some inconsistencies could occur throughout the quantification of As oxidation states using the XPS analysis. Since it was demonstrated that exposure to X-ray during examination could trigger the reduction of As(III) species,[49] for this reason, a control experiment was conducted. The arsenate salt, the reagent used as the arsenate source for adsorption experiments, was analyzed using XPS measurements at the same conditions (Table S8†). It is realized that a small quantity (4.6%) of –As(III)–O is included in the sample. However, after arsenate adsorption, two As(III)–O signals may be due to a reduction triggered by the adsorption process because some DMF molecules might remain in the pores of DUT-5 then it is a strong electron-donating group and could have led to the reduction of As(V).[50]

A contribution at 134.1 eV is observed in the HRXPS P 2p spectrum related to –P(V)–O. In addition, changes in HRXPS Al 2p spectra are noticed. Pristine DUT-5 displays a peak in Al $2p_{3/2}$ at 74.5 eV. After adsorption, the peak shifted to a higher value at 74.7 eV for both pollutants. The low 0.2 eV displacement of Al 2p binding energy is strongly induced by the electron density enhancement surrounding the Al ions. This can be associated with a hydrogen bonding interaction through weak Lewis acid–base interactions during adsorption.[51,52] Furthermore, a slight change is observed in the O 1s signals (Table S10†) after arsenate removal for Al–O contribution. For phosphate adsorption, three peaks at 530.4, 531.7, and 532.6 eV correspond to –Al–O, –C═O, and –C–O–H, respectively, display a slight 0.1 eV shift from the pristine material. While hydrogen bonding was more prominent for the phosphate removal, as observed in the pH study, it was observed that the electrostatic interaction was involved in the arsenate adsorption mechanism.[53] The signal's effects confirmed these changes in C 1s (Table S11†). The peak at 284.1 eV, related to the –C═C aromatic ring, shifts to 284.3 eV, while arsenate remains unchanged. Also, two peaks at 286.0 and 288.9 eV corresponded to –C–O and –C═O, respectively, turning 0.3 and 0.2 eV for arsenate removal and 0.6 and 0.1 eV for phosphate removal, respectively. These modifications are due to electrostatic forces already existing during arsenate adsorption.[28,38,54] In addition, these results are in agreement with the FTIR data since no apparent changes are observed, and with the low $\Delta H°$ value for arsenate adsorption and a higher for phosphate adsorption.

Reusability studies

Furthermore, the regeneration process is one of the main keys to sustainability in practical application. DUT-5 was exposed for three adsorption–desorption cycles in phosphate and arsenate adsorption, using 0.01 M HCl and 0.01 M $NaHCO_3$ as desorbing agents, respectively (Fig. 6). The adsorption capacity only drops 10 mg g^{-1} after the three adsorption–desorption cycles for phosphate. Representing that DUT-5 retained 80% of its original adsorption capacity. It is observed to have an excellent performance for phosphate adsorption over various cycles. However, in the case of arsenate adsorption cyclability performance, DUT-5 shows a poor adsorption capacity after three adsorption–desorption cycles, dropping to 1.21 mg g^{-1}. These behaviors were assumed by crystalline structural damage after the cyclin process, which was confirmed by PXRD analysis (Fig. S12 and S13†). Moreover, an irreversible adsorption process is noted

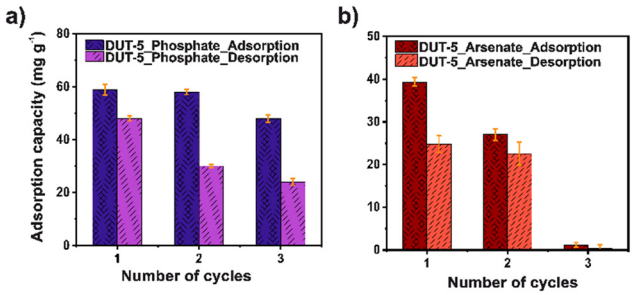

Fig. 6 Cycles of reusing DUT-5 adsorbent for adsorption of a) phosphate and b) arsenate from water.

 © 2024 The Author(s). Published by the Royal Society of Chemistry

Open Access Article. Published on 25 Fankwa-b 2023. Downloaded on 2025/10/07 3:46:55 AM.
This article is licensed under a Creative Commons Attribution 3.0 Unported Licence.

since the adsorption sites remain occupied for the pollutants molecules, which alters the crystalline structure of DUT-5.[55] It is probably due to the interference of the oxo-anions (arsenate and phosphate) with the coordination center between the Al^{3+} ions and the bpdc linkers. It was reported that high oxo-anion concentrations with low pK_a (phosphate and arsenate) values degradates the crystalline structure of a carboxyl-based MOF.[56] In this case, ppm concentration levels were employed for the adsorption studies. However, oxo-anions remained within the pores after the reusability process, increasing the oxo-anions concentration. This is directly related to the loss of the crystalline structure.

Conclusions

In this study, a water-stable Al(III)-based MOF DUT-5 was synthesized using a solvothermal method to selectively capture arsenate and phosphate from an aqueous solution. DUT-5 displays high stability and excellent adsorption performance from pH 4 to 9 for phosphate removal. The coexisting interfering ions in water exhibited no significant impact on phosphate adsorption and arsenate. Moreover, DUT-5 displays high selectivity for phosphate and excellent recyclability. Furthermore, the maximum Langmuir adsorption capacities for phosphate and arsenate were 233.26 and 131.32 mg g^{-1}, respectively, outperforming some related MOFs reported in the literature. The adsorption process and kinetics follow PSO and Freundlich models for both pollutants, driven by a diffusion mechanism on a heterogeneous surface involving chemical forces. Additionally, the possible mechanism was supported by FTIR and XPS analysis. It was demonstrated that hydrogen bonding and electrostatic interactions are presented for arsenate and hydrogen bonding for phosphate removal. Thus, DUT-5 encourages applications for phosphate and arsenate sequestration in water treatment.

Conflicts of interest

There are no conflicts to declare.

Acknowledgements

J. L. O. thanks CONAHCYT for the Ph.D. fellowship (1003953). I. A. I. thanks PAPIIT UNAM (IN201123), México, for financial support. C. L. thanks to the IPN-SIP project (20231282). We thank U. Winnberg (Euro Health) for scientific discussions and G. Ibarra-Winnberg for scientific encouragement.

References

1 V. Sharma, M. Sharma, S. Pandita, V. Kumar, J. Kour and N. Sharma, in *Heavy Metals in the Environment*, Elsevier, 2021, pp. 165–178.
2 F. D. Owa, *Mediterr. J. Soc. Sci.*, 2013, **4**, 1–6.
3 K. L. Wasewar, S. Singh and S. K. Kansal, in *Inorganic Pollutants in Water*, Elsevier, 2020, pp. 245–271.
4 L. Herrera-Estrella and D. López-Arredondo, *Trends Plant Sci.*, 2016, **21**, 461–463.
5 B. K. Mandal and K. T. Suzuki, *Talanta*, 2002, **58**, 201–235.
6 C. R. Tyler and A. M. Allan, *Curr. Environ. Health Rep.*, 2014, **1**, 132–147.
7 D. A. Lemley and J. B. Adams, in *Encyclopedia of Ecology*, Elsevier, 2019, pp. 86–90.
8 M. Baxa, M. Musil, M. Kummel, P. Hanzlík, B. Tesařová and L. Pechar, *Sci. Total Environ.*, 2021, **766**, 142647.
9 M. Arabnezhad, M. Shafiee Afarani and A. Jafari, *Int. J. Environ. Sci. Technol.*, 2019, **16**, 463–468.
10 K. C. Khulbe and T. Matsuura, *Appl. Water Sci.*, 2018, **8**, 19.
11 K. S. Hashim, R. Al Khaddar, N. Jasim, A. Shaw, D. Phipps, P. Kot, M. O. Pedrola, A. W. Alattabi, M. Abdulredha and R. Alawsh, *Sep. Purif. Technol.*, 2019, **210**, 135–144.
12 R. Paz, H. Viltres, N. K. Gupta, K. Rajput, D. R. Roy, A. Romero-Galarza, M. C. Biesinger and C. Leyva, *J. Mol. Liq.*, 2022, **356**, 118957.
13 I. W. Almanassra, V. Kochkodan, G. Mckay, M. A. Atieh and T. Al-Ansari, *J. Environ. Manage.*, 2021, **287**, 112245.
14 M. Hermassi, C. Valderrama, N. Moreno, O. Font, X. Querol, N. Batis and J. L. Cortina, *J. Chem. Technol. Biotechnol.*, 2016, **91**, 1962–1971.
15 A. Humayro, H. Harada and K. Naito, *J. Agric. Chem. Environ.*, 2021, **10**, 80–90.
16 H.-C. Zhou and S. Kitagawa, *Chem. Soc. Rev.*, 2014, **43**, 5415–5418.
17 S. L. James, *Chem. Soc. Rev.*, 2003, **32**, 276.
18 E. Medel, J. L. Obeso, C. Serrano-Fuentes, J. Garza, I. A. Ibarra, C. Leyva, A. K. Inge, A. Martínez and R. Vargas, *Chem. Commun.*, 2023, **59**, 8684–8687.
19 B. Wang, X.-L. Lv, D. Feng, L.-H. Xie, J. Zhang, M. Li, Y. Xie, J.-R. Li and H.-C. Zhou, *J. Am. Chem. Soc.*, 2016, **138**, 6204–6216.
20 J. L. Obeso, D. R. Amaro, C. V. Flores, A. Gutiérrez-Alejandre, R. A. Peralta, C. Leyva and I. A. Ibarra, *Coord. Chem. Rev.*, 2023, **485**, 215135.
21 V. B. López-Cervantes, D. W. Kim, J. L. Obeso, E. Martínez-Ahumada, Y. A. Amador-Sánchez, E. Sánchez-González, C. Leyva, C. S. Hong, I. A. Ibarra and D. Solis-Ibarra, *Nanoscale*, 2023, **15**, 12471–12475.
22 Y. Zhang, H. Liu, F. Gao, X. Tan, Y. Cai, B. Hu, Q. Huang, M. Fang and X. Wang, *EnergyChem*, 2022, **4**, 100078.
23 X. Liu, Y. Li, Z. Chen, H. Yang, Y. Cai, S. Wang, J. Chen, B. Hu, Q. Huang, C. Shen and X. Wang, *Crit. Rev. Environ. Sci. Technol.*, 2023, **53**, 1289–1309.
24 Z. Chen, Y. Li, Y. Cai, S. Wang, B. Hu, B. Li, X. Ding, L. Zhuang and X. Wang, *Carbon Research*, 2023, **2**, 8.
25 N. Assaad, G. Sabeh and M. Hmadeh, *ACS Appl. Nano Mater.*, 2020, **3**, 8997–9008.
26 J. Cai, X. Wang, Y. Zhou, L. Jiang and C. Wang, *Phys. Chem. Chem. Phys.*, 2016, **18**, 10864–10867.
27 J. Li, Y. Wu, Z. Li, M. Zhu and F. Li, *Water Sci. Technol.*, 2014, **70**, 1391–1397.
28 R. Liu, L. Chi, X. Wang, Y. Wang, Y. Sui, T. Xie and H. Arandiyan, *Chem. Eng. J.*, 2019, **357**, 159–168.

Open Access Article. Published on 25 Fankwa-b 2023. Downloaded on 2025/10/07 3:46:55 AM.
This article is licensed under a Creative Commons Attribution 3.0 Unported Licence.

29 W. Fan, K.-Y. Wang, C. Welton, L. Feng, X. Wang, X. Liu, Y. Li, Z. Kang, H.-C. Zhou, R. Wang and D. Sun, *Coord. Chem. Rev.*, 2023, **489**, 215175.
30 I. Senkovska, F. Hoffmann, M. Fröba, J. Getzschmann, W. Böhlmann and S. Kaskel, *Microporous Mesoporous Mater.*, 2009, **122**, 93–98.
31 J. L. Obeso, A. López-Olvera, C. V. Flores, E. Martínez-Ahumada, R. Paz, H. Viltres, A. Islas-Jácome, E. González-Zamora, J. Balmaseda, S. López-Morales, M. A. Vera, E. Lima, I. A. Ibarra and C. Leyva, *J. Mol. Liq.*, 2022, **368**, 120758.
32 J. L. Obeso, H. Viltres, C. V. Flores, A. López-Olvera, A. R. Rajabzadeh, S. Srinivasan, I. A. Ibarra and C. Leyva, *J. Environ. Chem. Eng.*, 2023, **11**, 109872.
33 W. W. Lestari, E. N. Afifah, O. Mohammed, T. E. Saraswati, R. Al-Adawiyah, G. T. M. Kadja and N. Widiastuti, *Mater. Res. Express*, 2020, **6**, 1250d4.
34 Y. Hu, M. Guo, S. Zhang, W. Jiang, T. Xiu, S. Yang, M. Kang, Z. Dongye, Z. Li and L. Wang, *Microporous Mesoporous Mater.*, 2022, **333**, 111740.
35 S. Zang, H. Qiu, C. Sun, H. Zhou and L. Cui, *Bull. Environ. Contam. Toxicol.*, 2022, **109**, 379–385.
36 Z. Wang, W. Hu, Z. Kang, X. He, Z. Cai and B. Deng, *Chem. Eng. J.*, 2019, **357**, 463–472.
37 Z. Yang, T. Zhu, M. Xiong, A. Sun, Y. Xu, Y. Wu, W. Shu and Z. Xu, *Inorg. Chem. Commun.*, 2021, **132**, 108804.
38 S. Su, R. Zhang, J. Rao, J. Yu, X. Jiang, S. Wang and X. Yang, *J. Environ. Chem. Eng.*, 2022, **10**, 108527.
39 M. H. Hassan, R. Stanton, J. Secora, D. J. Trivedi and S. Andreescu, *ACS Appl. Mater. Interfaces*, 2020, **12**, 52788–52796.
40 M. Li, Y. Liu, F. Li, C. Shen, Y. V. Kaneti, Y. Yamauchi, B. Yuliarto, B. Chen and C.-C. Wang, *Environ. Sci. Technol.*, 2021, **55**, 13209–13218.
41 Z. Lin, J. Tang, X. Huang and J. P. Chen, *Chemosphere*, 2022, **292**, 133498.
42 S. Rahdar, M. Taghavi, R. Khaksefidi and S. Ahmadi, *Appl. Water Sci.*, 2019, **9**, 87.
43 F.-C. Wu, R.-L. Tseng and R.-S. Juang, *Chem. Eng. J.*, 2009, **153**, 1–8.
44 W. Yu, M. Luo, Y. Yang, H. Wu, W. Huang, K. Zeng and F. Luo, *J. Solid State Chem.*, 2019, **269**, 264–270.
45 J. Sun, X. Zhang, A. Zhang and C. Liao, *J. Environ. Sci.*, 2019, **80**, 197–207.
46 L. Kang, M. Mucci and M. Lürling, *Sci. Total Environ.*, 2022, **812**, 151489.
47 M. N. Sahmoune, *Environ. Chem. Lett.*, 2019, **17**, 697–704.
48 T. Liu, S. Zheng and L. Yang, *J. Colloid Interface Sci.*, 2019, **552**, 134–141.
49 H. Viltres, O. F. Odio, L. Lartundo-Rojas and E. Reguera, *Appl. Surf. Sci.*, 2020, **511**, 145606.
50 T. Yao, H. Zou, J. Zhang and Y. Zhou, *J. Mater. Sci.: Mater. Electron.*, 2021, **32**, 26905–26916.
51 D. Chen, H. Yu, M. Pan and B. Pan, *Chem. Eng. J.*, 2022, **433**, 133690.
52 Y. Wang, W. Zhao, Z. Qi, L. Zhang and Y. Peng, *Sci. Total Environ.*, 2020, **745**, 141054.
53 Z.-J. Lin, H.-Q. Zheng, Y.-N. Zeng, Y.-L. Wang, J. Chen, G.-J. Cao, J.-F. Gu and B. Chen, *Chem. Eng. J.*, 2019, **378**, 122196.
54 C. Yin, S. Li, L. Liu, Q. Huang, G. Zhu, X. Yang and S. Wang, *J. Mol. Liq.*, 2022, **346**, 117101.
55 S. Li, T. Lei, F. Jiang, M. Liu, Y. Wang, S. Wang and X. Yang, *J. Colloid Interface Sci.*, 2020, **560**, 321–329.
56 W. Zhang, A. Bu, Q. Ji, L. Min, S. Zhao, Y. Wang and J. Chen, *ACS Appl. Mater. Interfaces*, 2019, **11**, 33931–33940.

© 2024 The Author(s). Published by the Royal Society of Chemistry